Environmental Engineering Research

Environ. Eng. Res. 2012 December,17(4) : 179-184

Research Paper

http://dx.doi.org/10.4491/eer.2012.17.4.179
pISSN 1226-1025 eISSN 2005-968X

Control of Methyl Tertiary-Butyl Ether via Carbon-Doped Photocatalysts under Visible-Light Irradiation

Joon-Yeob Lee, Wan-Kuen Jo†

Department of Environmental Engineering, Kyungpook National University, Daegu 702-701, Korea

Abstract

The light absorbance of photocatalysts and reaction kinetics of environmental pollutants at the liquid-solid and gas-solid interfaces differ from each other. Nevertheless, many previous photocatalytic studies have applied the science to aqueopus applications without due consideration of the environment. As such, this work reports the surface and morphological characteristics and photocatalytic activities of carbon-embedded (C-TiO_2) photocatalysts for control of gas-phase methyl tertiary-butyl ether (MTBE) under a range of different operational conditions. The C-TiO_2 photocatalysts were prepared by oxidizing titanium carbide powders at 350°C. The characteristics of the C-TiO_2 photocatalysts, along with pure TiC and the reference pure TiO_2, were then determined by X-ray diffraction, scanning emission microscope, diffuse reflectance ultraviolet-visible-near infrared (UV-VIS-NIR), and Fourier transform infrared spectroscopy. The C-TiO_2 powders showed a clear shift in the absorbance spectrum towards the visible region, which indicated that the C-TiO_2 photocatalyst could be activated effectively by visible-light irradiation. The MTBE decomposition efficiency depended on operational parameters, including the air flow rate (AFR), input concentration (IC), and relative humidity (RH). As the AFRs decreased from 1.5 to 0.1 L/min, the average efficiencies for MTBE increased from 11% to 77%. The average decomposition efficiencies for the ICs of 0.1, 0.5, 1.0, and 2.0 ppm were 77%, 77%, 54%, and 38%, respectively. In addition, the decomposition efficiencies for RHs of 20%, 45%, 70%, and 95% were 92%, 76%, 50%, and 32%, respectively. These findings indicate that the prepared photocatalysts could be effectively applied to control airborne MTBE if their operational conditions were optimized.

Keywords: Air flow rate, Input concentration, Relative humidity, Titanium carbide, Visible light

1. Introduction

Methyl tertiary-butyl ether (MTBE) has received a great deal of attention over recent years due to its widespread detection in indoor environments, including residential buildings and vehicle interiors. MTBE is added to unleaded gasoline to increase the octane rating and enhance combustion efficiency [1, 2]. The addition of MTBE to unleaded gasoline reduces atmospheric CO emission levels by 10−15% [3], however, it is toxic in its own right and building and vehicle occupants are exposed to it through its addition to fuel [1, 2]. Previous studies [4, 5] have reported that MTBE concentrations may be higher in residences than outdoors as a result of the atmospheric containment of sources of MTBE. A major source of MTBE in such instances may include automobiles at parking areas adjacent to buildings and garages, where vehicle emissions can penetrate into the building interior. The vehicle cabin is also a contained environment associated with elevated personal exposure to MTBE [6]. MTBE is a potential carcinogen and causes other adverse health effects, such as dizziness, nausea, eye irritation, and headache [7]. These characteristics of MTBE along with its prevalence around humans have prompted the development of control measures to lower health risks of building and vehicle occupants from indoor exposure.

Heterogeneous photocatalysis using semiconductors is considered to be a viable tool for the treatment of air and water pollution. Among various semiconductors, titanium dioxide (TiO_2) has primarily been used for the photocatalytic control of water and air pollutants due to its outstanding photocatalytic performance and stability toward photocorrosion [8]. The photocatalytic process converts light energy into chemical energy. However, because of its high band gap energy (3.2 eV), this process requires UV light irradiation <387 nm to generate electron-hole pairs [7]. Many researchers have attempted to modify TiO_2 to improve its light absorption capacity and photocatalytic oxidation efficiency under visible-light irradiation conditions using cocatalytic process, dye sensitization, metallic embedding, metal particle loading, and nonmetallic embedding [9-14].

Carbon-doped TiO_2 (C-TiO_2) is a prospective heterogeneous photocatalyst that is enhanced by nonmetallic doping techniques, because C-TiO_2 photocatalysts effectively extend the light absorbance into the visible region due to their unique electrical and structural properties [13]. Several researchers have prepared

Received August 24, 2012 **Accepted** October 23, 2012

†Corresponding Author
E-mail: wkjo@knu.ac.kr
Tel: +82-53-950-6584 Fax: +82-53-950-6579

C-TiO_2 photocatalysts using a variety of synthesis processes, including chemical vapor deposition, thermal oxidation of titanium carbide, sol-gel processes, and hydrothermal methods [15-19]. These studies have revealed that C-TiO_2 photocatalysts have high photocatalytic performance under visible-light irradiation conditions. For these studies, photocatalytic performance tests were primarily carried out in the aqueous phase to investigate the decomposition of water pollutants such as 4-chlorophenol, dye reactive brilliant red X-3B, methyl orange, methylene blue, phenol, rhodamine B, and trichloroacetic acid. However, the light absorbance of photocatalysts and reaction kinetics of environmental pollutants differ at the liquid-solid and gas-solid interfaces. For gas-solid photocatalytic reactions, the photocatalytic performance primarily depends on the concentrations and types of gas-phase compounds, air flow rate (AFR), light intensity, and humidity. Conversely, the major parameters associated with liquid-solid photocatalytic reactions involve ions, pH, concentrations, types of water pollutants, and light intensity [8]. These differences imply that the photocatalytic performance obtained from aqueous-phase applications may not be calculated based on data from gas-phase applications. In order to more accurately estimate the performance of such systems, this study assessed the photocatalytic activities of C-TiO_2 photocatalysts for purification of gas-phase MTBE under different experimental conditions. MTBE was chosen as a target pollutant based on its prevalence in vehicle interiors and its toxicity [6, 7].

2. Materials and Methods

2.1. Preparation and Characterization of Photocatalysts

Titanium carbide (TiC) powders were purchased from Taiji-Ring Co., China and were oxidized at 350°C to prepare C-TiO_2 photocatalysts. TiC powders were sprayed uniformly onto a glass plate and were then oxidized at the specified temperature (350°C) for 8 hr to give grey powders [16]. The prepared powders, along with pure TiC powders and reference Degussa P25 pure TiO_2 powders, were then characterized by X-ray diffraction (XRD), scanning emission microscope (SEM), diffuse reflectance ultraviolet-visible-near infrared (UV-VIS-NIR), and/or Fourier transform infrared (FTIR) spectroscopy. XRD patterns were measured using a Rigaku D/max-2500 diffractometer with Cu K_α radiation operated at 40 kV and 100 mA. The powder morphology was observed using the Hitachi S-4300 and EDX-350 field emission (FE)-SEM at an acceleration voltage of 15 kV. Visible absorption spectra were identified using a Varian CARY 5G spectrophotometer equipped with an integrating sphere. FTIR analysis was conducted using a PerkinElmer Spectrum GX spectrophotometer at a resolution of 4/cm in the spectral range of 400–4,000/cm.

2.2. Photocatalytic Performance Test

The photocatalytic performances of the photocatalysts were examined using a cylindrical photocatalytic reactor, which was prepared using a Pyrex tube with a 4.5 cm inside diameter and a length of 26.5 cm [20]. The inner surface of the reactor was coated with the C-TiO_2 photocatalyst. To accomplish this, the powders were ground in a ceramic bowl and were mixed with 0.1 M aqueous EDTA solution, after which deionized water was added to dilute the mixture. Subsequently, Triton X-100 was added and the mixture was pasted onto the Pyrex reactor. The pasted reactor was then dried at 100°C for 30 min and was then calcined in an oven for a further 30 min at the same temperature that was used for its oxidation.

A daylight lamp with a geometry that allowed for uniform light distribution onto the surfaces of the photocatalysts was inserted inside the coated reactor, and the outside of the reactor was wrapped with aluminum foil to prevent light loss from the reactor lamp through the Pyrex reactor window, as well as to stop the influx of light from external sources. The standard gas was prepared by injecting MTBE into a mixing apparatus using a syringe pump (KDS210; KD Scientific, Holliston, MA, USA) and by mixing with humidified air. This gas flowed above the photocatalyst-coated Pyrex reactor. The humidity level was controlled by making zero-grade air pass through an activated carbon filter, followed by water-contained impingers in a water bath. The relative humidity (RH) was monitored adjacent to the photocatalytic reactor inlet and outlet using a humidity meter. AFR was adjusted using both rotameters and a mass-flow meter.

The photocatalytic activities of the photocatalysts were examined under different conditions on the basis of AFRs, input concentrations (ICs), and RHs. The AFR range for these experiments was set at 0.1–1.0 L/min (0.1, 0.3, 0.5, and 1.0 L/min), covering a broad range. The ICs ranged from 0.1–2.0 ppm (0.1, 0.5, 1.0, and 2.0 ppm), which included in-vehicle concentration levels [2]. The RH was adjusted to 20–95% (20%, 45%, 70%, and 95%) to cover both dry and humidified environmental conditions. For the test of each parameter, other parameters were fixed to their representative values: AFR, 0.5 L/min; IC, 0.1 ppm; and RH, 45%. Visible-light radiation was provided using an 8-W fluorescent daylight lamp (F8T5DL; Youngwha Lamp Co., Seoul, Korea). The spectrum of this light source was 400–720 nm. Its intensity was determined to be 2.1 mW/cm^2, at a distance from the visible-light lamp equal to half the hydraulic diameter (HD, 1.0 cm) – defined as the inside diameter of the annular reactor tube, minus the outside diameter of the lamp – of the reactor, by using a digital Lux meter (DX-100; INS Enterprise, Taipei, Taiwan). Although the daylight lamp used in this study irradiated UVA light at 0.1 mW/cm^2, the commercially-available daylight lamp was used as a light source for practical photocatalytic applications, instead of pure visible-light source. The coating weight of the C-TiO_2 photocatalyst was approximately 3.3 mg/cm^2. For comparison, the current study additionally investigated the plug-flow reactor coated with pure TiC under the representative experimental conditions.

Air sampling was carried out by filling a clean Tedlar bag at both the reactor inlet and outlet for 10 min with a specified time interval. The collected chemical species were analyzed using a gas chromatographer (Agilent 7890) with a fused silica column (Supelco SPB-5) which was coupled with a flame ionization detector. The peak areas for compounds other than MTBE on the chromatogram were negligible; thus, they were neither qualified nor quantified. The quality control program for the measurements of MTBE involved laboratory blank and spiked samples. The method detection limit of MTBE was 1.2 ppb.

3. Results and Discussion

3.1. Characteristics of the Prepared Photocatalysts

The characteristics of pure TiC, C-TiO_2, and the reference pure TiO_2 were determined utilizing XRD, Fig. 1. SEM, UV-VIS-

NIR, and FTIR spectroscopy. When applied to analysis by XRD, pure TiC exhibited several TiC-associated peaks, but not any TiO_2-associated peaks, such as anatase and rutile crystal phases. This indicates that TiO_2 crystal phases were not included in the TiC. In contrast, C-TiO_2 showed not only one TiC-related peak at 36.5° 2θ, but also an anatase titania phase with a distinct peak at 25.2° 2θ and a rutile titania phase with a distinct peak at 27.4° 2θ.

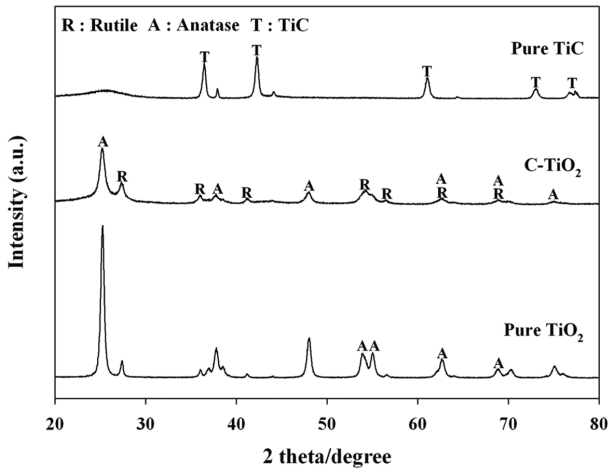

Fig. 1. X-ray diffraction spectra of titanium carbide (TiC), carbon-doped TiO_2 (C-TiO_2), and pure titanium dioxide (TiO_2).

For the C-TiO_2, the peak which appeared at 36.0° 2θ is likely due to the overlap of TiC and TiO_2 rutile phase, while the other peaks are attributed to anatase or rutile phases [18, 21]. In addition, it is noteworthy that the peak intensity of the rutile crystal phase was stronger for C-TiO_2 than for pure TiO_2, whereas the reverse was true for the anatase crystal phase, providing a higher rutile-to-anatase ratio for the C-TiO_2. Consequently, it was confirmed that TiO_2 crystal phases were formed during the oxidation of TiC at high temperature conditions.

Fig. 2 shows the SEM images of pure TiC, C-TiO_2, and the reference pure TiO_2. The sizes of agglomerated particles were similar for pure TiC and C-TiO_2, indicating that the synthesis process for C-TiO_2 by oxidizing TiC does not change the size of particles. However, the sizes of agglomerated particles were larger for C-TiO_2 than the reference pure TiO_2. As demonstrated by the XRD results, C-TiO_2 exhibited a higher rutile-to-anatase ratio as compared with the pure TiO_2. In addition, the crystallite size of rutile phase is generally larger than that of anatase phase [22]. Accordingly, the larger particle size for the C-TiO_2 is ascribed to the rutile phase crystal phase with larger particle sizes.

Fig. 3 shows the UV-visible absorption spectra of pure TiC, C-TiO_2, and the reference pure TiO_2. The P25 TiO_2 revealed an absorption edge at $\lambda \approx 420$ nm, which was consistent with that reported by other researchers [20, 23]. In contrast, absorption edge of pure TiC and C-TiO_2 shifted to the visible-light range. The optical absorption thresholds for both types of powders were >700 nm. For C-TiO_2, the absorption shift to the visible-light range were attributed to the presence of carbonate species at interstitial positions of TiO_2 lattice [19]. Similarly, previous studies

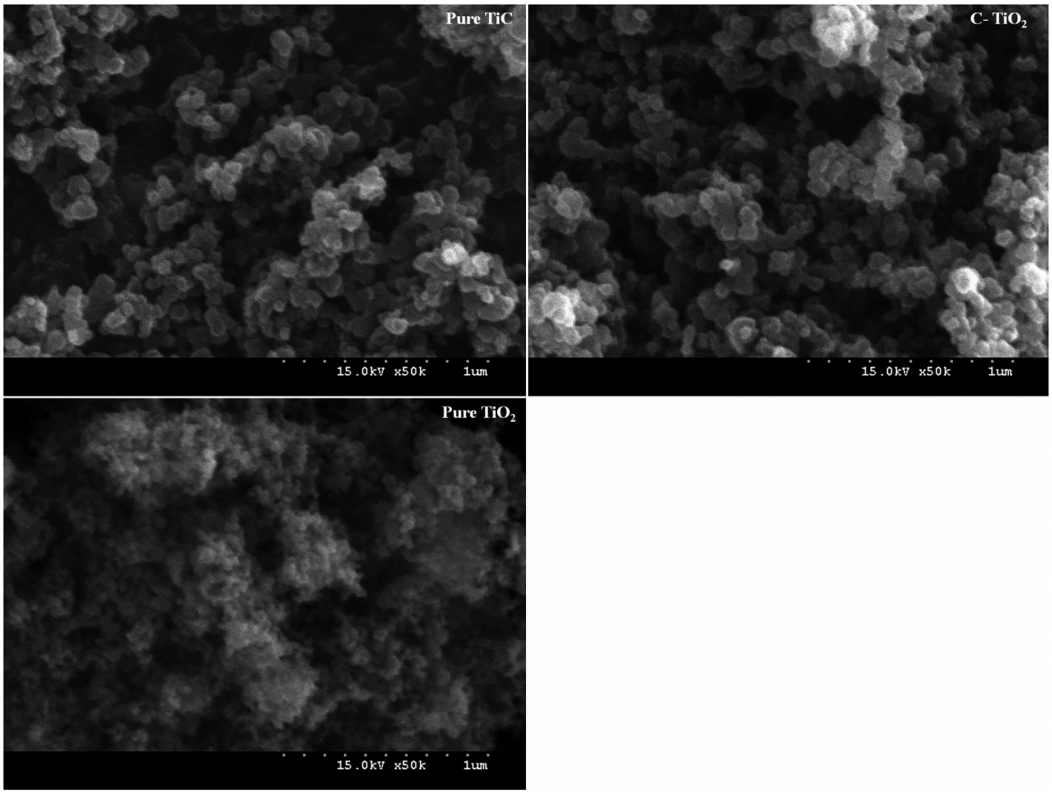

Fig. 2. Scanning electron microscope pattern of titanium carbide (TiC), carbon-doped TiO_2 (C-TiO_2), and pure titanium dioxide (TiO_2).

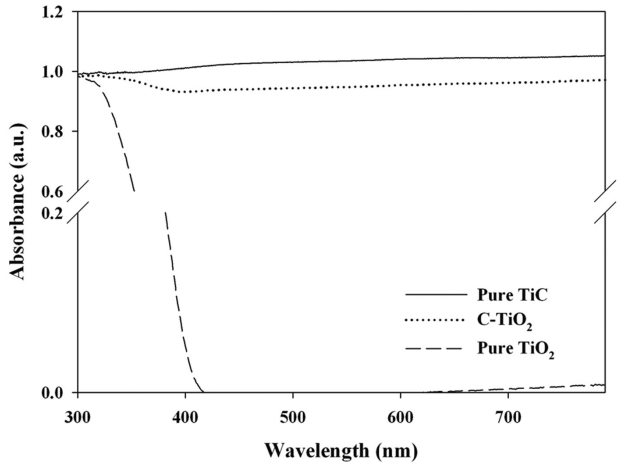

Fig. 3. UV-visible absorption spectra of titanium carbide (TiC), carbon-doped TiO_2 (C-TiO_2), and pure titanium dioxide (TiO_2).

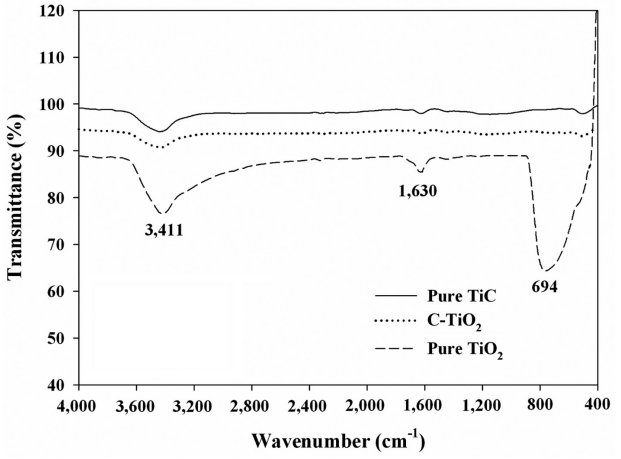

Fig. 4. Fourier transform infrared spectra of titanium carbide (TiC), carbon-doped TiO_2 (C-TiO_2), and pure titanium dioxide (TiO_2).

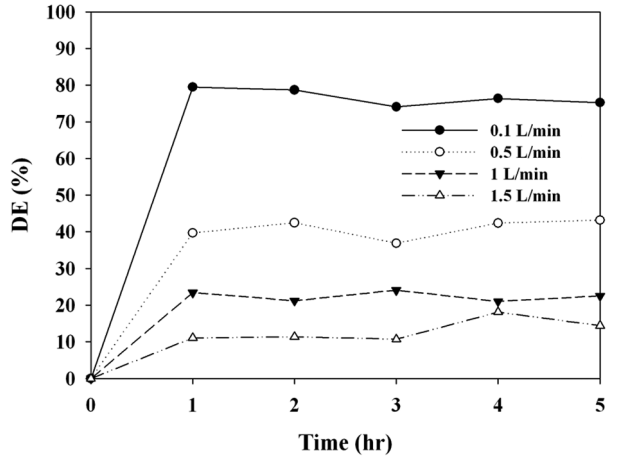

Fig. 5. Methyl tertiary-butyl ether decomposition efficiency (DE, %) of photocatalytic systems with carbon-doped TiO_2 (C-TiO_2) photocatalyst according to air flow rate (0.1, 0.5, 1.0, and 1.5 L/min).

[19, 21] reported that the C-TiO_2 photocatalysts prepared using other synthetic routes showed a light absorbance shift to the visible-light region, although their absorbance intensities differed. As such, these findings suggest that the C-TiO_2 photocatalysts y could be activated under visible-light range.

The FTIR spectra of pure TiC, C-TiO_2, and the reference pure TiO_2 are presented in Fig. 4. Two bands at 3,440/cm and 1,626/cm were appeared for the pure TiC as well as C-TiO_2 and pure TiO_2. The band at 3,440/cm corresponds to the O-H stretching vibration, whereas the band at 1,626/cm results from O-H bending of adsorbed water molecules [21, 24]. Other bands below were also observed for the oxidized photocatalysts, whereas they were negligibly observed for the TiC. These bands were ascribed to the titania crystal lattice vibration [25]. However, the bands at 460 and 694 nm, which were assigned to the stretching vibration of Ti–O [26], were much stronger for pure TiO_2 than for pure TiC or C-TiO_2. Moreover, for the peak at <1,000/cm the frequency was shifted from 694 nm for TiO_2 to lower values for C-TiO_2. This frequency movement to a lower wavelength for C-TiO_2 is likely due to the interaction between the impregnated C atoms.

3.2. Control Efficiencies of C-TiO_2 Photocatalysts

The control efficiencies for MTBE determined via prepared C-TiO_2 photocatalysts were investigated under a range of operational conditions, which were determined on the basis of three parameters (IC, AFR, and RH). Fig. 5 shows the photocatalytic decomposition efficiency for MTBE determined via the C-TiO_2 according to AFRs. Similar to other photocatalytic studies [27, 28], the MTBE decomposition efficiency decreased with increasing AFRs. As the AFRs was increased from 0.1 to 1.5 L/min, the average efficiencies for MTBE decreased from 77% to 11%, suggesting that AFR was still an important parameter for the photocatalytic decomposition mechanism of the C-TiO_2 system. As AFR was increased, the bulk mass transport of target compounds from the gas-phase to the surface of the catalyst particle, which is an important heterogeneous catalytic reaction process, would be increased mainly due to convection and diffusion [29]. As such, the decomposition rate would increase as AFR was increased, indicating that MTBE decomposition is limited to the mass transfer to C-TiO_2 surface. However, this pattern is in contrast to that determined in the current study. At higher AFRs the gas retention time in the photocatalytic reactor would be too short to provide sufficient MTBE transfer from the gas phase to the solid catalyst surface [29, 30]. The gas retention times in the current study were 76, 15.2, 7.6, and 3.8 sec for AFRs of 0.1, 0.5, 1.0, and 1.5 L/min, respectively. They were determined by dividing the photocatalytic reactor volume by AFR. Consequently, the lower efficiencies at higher AFRs indicate that an insufficient reactor retention time effect would exceed the bulk mass transport effect on MTBE decomposition on the catalyst surfaces. Meanwhile, our preliminary study showed that photocatalytic MTBE decomposition by Degussa P25 TiO_2 under visible-light was negligible.

Fig. 6 exhibits the photocatalytic MTBE decomposition efficiency of C-TiO_2, as determined according to the ICs. The decomposition efficiencies did not vary significantly with increasing IC within the range of 0.1–1.0 ppm. The average decomposition efficiencies for the ICs of 0.1, 0.5, 1.0, and 2.0 ppm were 77%, 77%, 54%, and 38%, respectively. This suggests that within this concentration range photocatalytic decomposition would occur on the C-TiO_2 surface through a Langmuir-Hinshelwood mechanism via first-order reaction kinetics. In contrast, Jo and

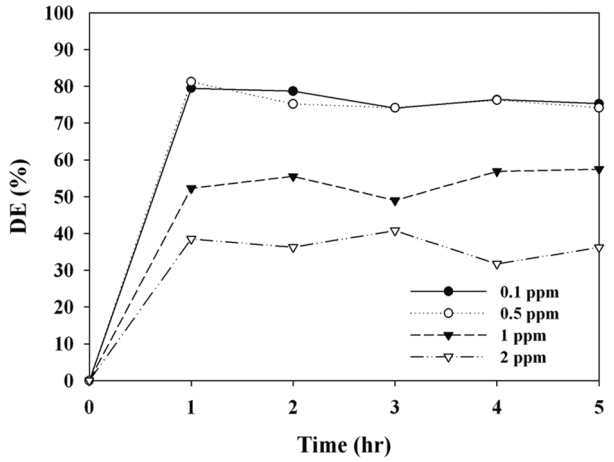

Fig. 6. Methyl tertiary-butyl ether decomposition efficiency (DE, %) of photocatalytic systems with carbon-doped TiO_2 (C-TiO_2) photocatalyst according to initial concentration (0.1, 0.5, 1.0, and 2.0 ppm).

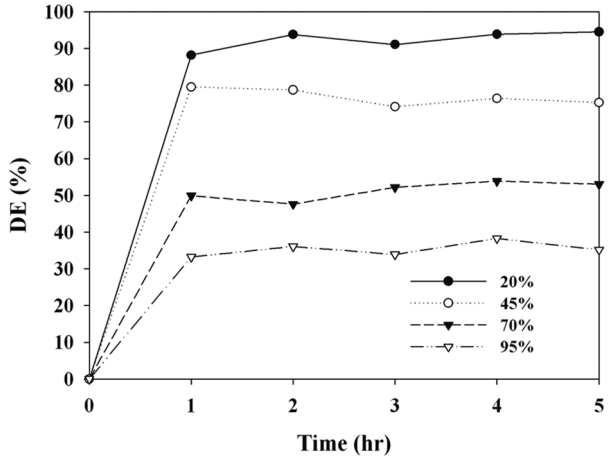

Fig. 7. Methyl tertiary-butyl ether decomposition efficiency (DE, %) of photocatalytic systems with carbon-doped TiO_2 (C-TiO_2) photocatalyst according to relative humidity (20%, 45%, 70%, and 95%).

Yang [31] determined the degradation efficiencies for benzene, toluene, ethylbenzene, and xylene (BTEX) using Degussa P25 TiO_2 under UV irradiation, reporting that the BTEX degradation efficiencies decreased gradually with increasing IC from 0.1 to 1.0 ppm, which covers the typical indoor air quality (IAQ) levels [2]. As such, it is further indicated that, unlike the stand-alone TiO_2, the photocatalytic performance of TiO_2 coupled with multi-wall carbon nanotubes for the decomposition of toxic gas-phase pollutants is not affected by changes in concentration within the simulated IAQ concentration range. The adsorption rate on the photocatalyst surface is an important parameter in determining photocatalytic degradation efficiencies [31]. Thus, the IC dependence determined in the present study was ascribed to competition between contaminant molecules for adsorption onto the catalyst surface.

Fig. 7 exhibits the photocatalytic decomposition efficiency for MTBE determined via the C-TiO_2 according to RH. The MTBE decomposition efficiency decreased with increasing RH. The average decomposition efficiencies for 20%, 45%, 70%, and 95% were 92%, 76%, 50%, and 32%, respectively. This pattern was consistent with that of other types of photocatalysts reported by other studies [20, 32]. For example, Sleiman et al. [32] reported that using low IC conditions (0.02–0.4 ppm), the toluene decomposition efficiency decreased with increasing RH within the RH range of 55–95%. With respect to high RH conditions, excessive water molecules would preferably occupy active sites on the photocatalyst surface, causing a decrease in the reaction rate. Therefore, it is suggested that like other types of photocatalysts, the photocatalytic decomposition efficiency of C-TiO_2 depends on RH.

4. Conclusions

This work determined the morphology and the photocatalytic activities of C-TiO_2 photocatalysts for the control of gas-phase MTBE under a range of different environmental conditions. The surface and morphological of C-TiO_2 could be successfully determined. A number of C-TiO_2 photocatalysts with different photocatalytic characteristics were prepared, and were analyzed for their relative activity alongside commercially available TiO_2 photocatalysts. The C-TiO_2 powders showed a clear shift in the absorbance spectrum towards the visible region, which indicates that the C-TiO_2 photocatalyst could be activated effectively by visible-light irradiation. The efficiency of MTBE decomposition depended on the operational parameters, such as AFR, IC, and RH. It is further suggested that C-TiO_2 photocatalysts could be effectively applied for airborne MTBE purification inside vehicles if their operational conditions are optimized.

Acknowledgments

This work was supported by the National Research Foundation of Korea (NRF) grant funded by the Korean government (MEST; No. 2011-0027916).

References

1. Lee JW, Jo WK. Actual commuter exposure to methyl-tertiary butyl ether, benzene and toluene while traveling in Korean urban areas. *Sci. Total Environ*. 2002;291:219-228.
2. Jia C, D'Souza J, Batterman S. Distributions of personal VOC exposures: a population-based analysis. *Environ. Int*. 2008;34:922-931.
3. Mannino DM, Etzel RA. Are oxygenated fuels effective? An evaluation of ambient carbon monoxide concentrations in 11 western states, 1986 to 1992. *J. Air Waste Manag. Assoc*. 1996;46:20-24.
4. Dodson RE, Levy JI, Spengler JD, Shine JP, Bennett DH. Influence of basements, garages, and common hallways on indoor residential volatile organic compound concentrations. *Atmos. Environ*. 2008;42:1569-1581.
5. Hun DE, Corsi RL, Morandi MT, Siegel JA. Automobile proximity and indoor residential concentrations of BTEX and MTBE. *Build. Environ*. 2011;46:45-53.
6. Geiss O, Tirendi S, Barrero-Moreno J, Kotzias D. Investigation

of volatile organic compounds and phthalates present in the cabin air of used private cars. *Environ. Int.* 2009;35:1188-1195.
7. US Environmental Protection Agency. Integrated Risk Information System (IRIS) [Internet]. Washington: US Environmental Protection Agency; c2012 [cited 2012 Dec 1]. Available from: http://www.epa.gov/iris/index.html.
8. Fujishima A, Zhang X, Tryk DA. TiO_2 photocatalysis and related surface phenomena. *Surf. Sci. Rep.* 2008;63:515-582.
9. Ding H, Sun H, Shan Y. Preparation and characterization of mesoporous SBA-15 supported dye-sensitized TiO_2 photocatalyst. *J. Photochem. Photobiol. A Chem*. 2005;169:101-107.
10. Li D, Haneda H, Hishita S, Ohashi N. Visible-light-driven nitrogen-doped TiO_2 photocatalysts: effect of nitrogen precursors on their photocatalysis for decomposition of gas-phase organic pollutants. *Mater. Sci. Eng. B* 2005;117:67-75.
11. Chen HW, Ku Y, Kuo YL. Effect of Pt/TiO_2 characteristics on temporal behavior of o-cresol decomposition by visible light-induced photocatalysis. *Water Res*. 2007;41:2069-2078.
12. Kuncewicz J, Zabek P, Stochel G, Stasicka Z, Macyk W. Visible light driven photocatalysis in chromate(VI)/TiO_2 systems: improving stability of the photocatalyst. *Catal. Today* 2011;161:78-83.
13. Leary R, Westwood A. Carbonaceous nanomaterials for the enhancement of TiO_2 photocatalysis. *Carbon* 2011;49:741-772.
14. Tian L, Zhao Y, He S, Wei M, Duan X. Immobilized Cu–Cr layered double hydroxide films with visible-light responsive photocatalysis for organic pollutants. *Chem. Eng. J.* 2012;184:261-267.
15. Kuo CS, Tseng YH, Huang CH, Li YY. Carbon-containing nano-titania prepared by chemical vapor deposition and its visible-light-responsive photocatalytic activit. *J. Mol. Catal. A Chem*. 2007;270:93-100.
16. Shen M, Wu Z, Huang H, Du Y, Zou Z, Yang P. Carbon-doped anatase TiO_2 obtained from TiC for photocatalysis under visible light irradiation. *Mater. Lett*. 2006;60:693-697.
17. Park Y, Kim W, Park H, Tachikawa T, Majima T, Choi W. Carbon-doped TiO_2 photocatalyst synthesized without using an external carbon precursor and the visible light activity. *Appl. Catal. B* 2009;91:355-361.
18. Ren W, Ai Z, Jia F, Zhang L, Fan X, Zou Z. Low temperature preparation and visible light photocatalytic activity of mesoporous carbon-doped crystalline TiO_2. *Appl. Catal. B* 2007;69:138-144.
19. Li H, Wang D, Fan H, Wang P, Jiang T, Xie T. Synthesis of highly efficient C-doped TiO(2) photocatalyst and its photogenerated charge-transfer properties. *J. Colloid Interface Sci.* 2011;354:175-180.
20. Jo WK, Kim JT. Application of visible-light photocatalysis with nitrogen-doped or unmodified titanium dioxide for control of indoor-level volatile organic compounds. *J. Hazard. Mater*. 2009;164:360-366.
21. Dong F, Wang H, Wu Z. One-step "green" synthetic approach for mesoporous C-doped titanium dioxide with efficient visible light photocatalytic activity. *J. Phys. Chem. C* 2009;113:16717-16723.
22. Wang X, Lim TT. Solvothermal synthesis of C–N codoped TiO_2 and photocatalytic evaluation for bisphenol A degradation using a visible-light irradiated LED photoreactor. *Appl. Catal. B* 2010;100:355-364.
23. Zand H, Kawase Y. Synthesis and characterization of S-doped Degussa P25 with application in decolorization of Orange II dye as a model substrate. *J. Mol. Catal. A Chem*. 2009;314:55-62.
24. Lin X, Rong F, Ji X, Fu D. Carbon-doped mesoporous TiO_2 film and its photocatalytic activity. *Microporous Mesoporous Mater.* 2011;142:276-281.
25. Peng T, Zhao D, Dai K, Shi W, Hirao K. Synthesis of titanium dioxide nanoparticles with mesoporous anatase wall and high photocatalytic activity. *J. Phys. Chem. B* 2005;109:4947-4952.
26. Nam SH, Kim TK, Boo JH. Physical property and photo-catalytic activity of sulfur doped TiO_2 catalysts responding to visible light. *Catal. Today* 2012;185:259-262.
27. Martinez T, Bertron A, Ringot E, Escadeillas G. egradation of NO using photocatalytic coatings applied to different substrates. *Build. Environ*. 2011;46:1808-1816.
28. Wang Z, Liu J, Dai Y, Dong W, Zhang S, Chen J. CFD modeling of a UV-LED photocatalytic odor abatement process in a continuous reactor. *J. Hazard. Mater*. 2012;215-216:25-31.
29. Bouzaza A, Vallet C, Laplanche A. Photocatalytic degradation of some VOCs in the gas phase using an annular flow reactor: determination of the contribution of mass transfer and chemical reaction steps in the photodegradation process. *J. Photochem. Photobiol. A Chem*. 2006;177:212-217.
30. Akly C, Chadik PA, Mazyck DW. Photocatalysis of gas-phase toluene using silica–titania composites: performance of a novel catalyst immobilization technique suitable for large-scale applications. *Appl. Catal. B* 2010;99:329-335.
31. Jo WK, Yang CH. Feasibility of a tandem photocatalytic oxidation-adsorption system for removal of monoaromatic compounds at concentrations in the sub-ppm-range. *Chemosphere* 2009;77:236-241.
32. Sleiman M, Conchon P, Ferronato C, Chovelon JM. Photocatalytic oxidation of toluene at indoor air levels (ppbv): Towards a better assessment of conversion, reaction intermediates and mineralization. *Appl. Catal. B* 2009;86:159-165.